

Booming dune instability

B. Andreotti and L. Bonneau

*Physique et Mécanique des Milieux Hétérogènes, UMR 7636 CNRS-ESPCI,
10 rue Vauquelin, 75231 Paris Cedex 05, France²*

(Dated: November 28, 2009)

Sand avalanches flowing down the leeward face of some desert dunes spontaneously produce a loud sound with a characteristic vibrato around a well defined frequency, a phenomenon called the "song of dunes". Here, we show through theory that a homogenous granular surface flow is linearly unstable towards growing elastic waves when a localized shear band forms at the interface between the avalanche and the static part of the dune. We unravel the nature of the acoustic amplifying mechanism at the origin of this booming instability. The dispersion relation and the shape of the most unstable modes are computed and compared to field measurements.

Many desert sand dunes emit a loud and harmonious sound as they avalanche, with large amounts of sand sliding down their slip faces. The first reports of this spontaneous acoustic emission in the scientific literature date back to the nineteenth century [1, 2]. This phenomenon has been extensively characterized in the field and the laboratory [3–6], but the cause has remained mysterious [7, 8]. The contradictory explanations previously proposed are based on different dynamical mechanisms: (i) The avalanche behaves as a quasi-periodic acoustic source due to stick-slip motion, a series of stop and go fronts [9, 10], or to the collisions between grains [11].

(ii) The avalanche is an incoherent broadband source but the emission frequency is selected by a resonance over either the thickness H of the avalanche [5] or the thickness of the dry layer at the surface of the dune [6]. The resonance, which is by definition a maximum of vibration amplitude, is due to the accumulation of energy in a standing wave. By contrast, for a propagative mode, the energy is radiated away from the source.

(iii) The avalanche acts as a selective acoustic amplifier based on the stimulated emission of surface elastic waves [4]. During the collision of grains inside the shear band separating the avalanche from the static part of the dune, energy is transferred from the shearing motion to elastic deformations. Conversely, coherent elastic modes [4, 12–14] tend to synchronize grain collisions: the probability that a collision takes place in phase with the vibration increases linearly with the amplitude of the later.

In the present letter, we propose an alternative explanation based on linear stability analysis of a homogeneous avalanche. Due to friction, the compressibility of the material cannot be neglected at low Mach number as it is coupled to the shear flow [18]. We show that the friction between the granular flow and the static part of the dune is responsible for an exponential growth of elastic waves. The connection between this instability and previous theoretical works published in the context of seismology [16, 17] and condensed matter physics [18] is discussed. Finally, our predictions are tested against field measurements performed during fifty controlled booming avalanches at Sidi-Aghfinir [4], in July 2009.

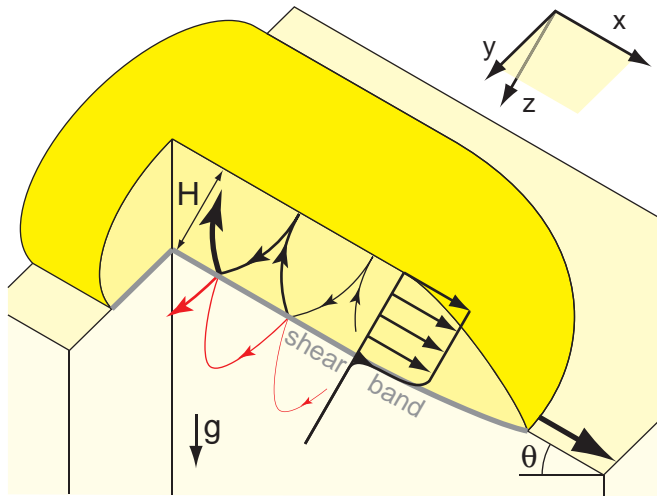


FIG. 1: Schematic diagram of a booming avalanche. Elastic waves are guided along the surface and amplified by reflections on the shear band when they propagate up the slope.

Steady state – Booming avalanches typically have a centimeter-scale thickness. Looking at the surface of such an avalanche from above, one observes a coherent solid-like motion over blocks as large as few tens of centimeters. This indicates a shear band localization, typical of granular flows just above the jamming transition [15]. Shear banding in booming flows has been witnessed directly in the field [6] and the lab [11]. As the shear band thickness is on the order of few grain diameters, it is much smaller than the acoustic wavelength at the booming frequency. Here, the avalanche is thus described as a plug flow separated from the static part of the dune by an infinitely small frictional shear band (fig. 1), characterized by a constant friction coefficient μ (μ is the ratio of the shear stress to the normal stress). In the steady state, the dune slope $\tan \theta$ must be equal to μ .

The vibrations in the two regions (avalanche and static part of the dune) in relative motion are described in the framework of non-linear elasticity. Starting from the coarse-grained displacement field \mathbf{U} , the strain tensor is defined as $u_{ij} = \frac{1}{2} \left(\frac{\partial U_i}{\partial x_j} + \frac{\partial U_j}{\partial x_i} \right)$. Assuming a non-linear Hertzian contact force between grains, the macroscopic

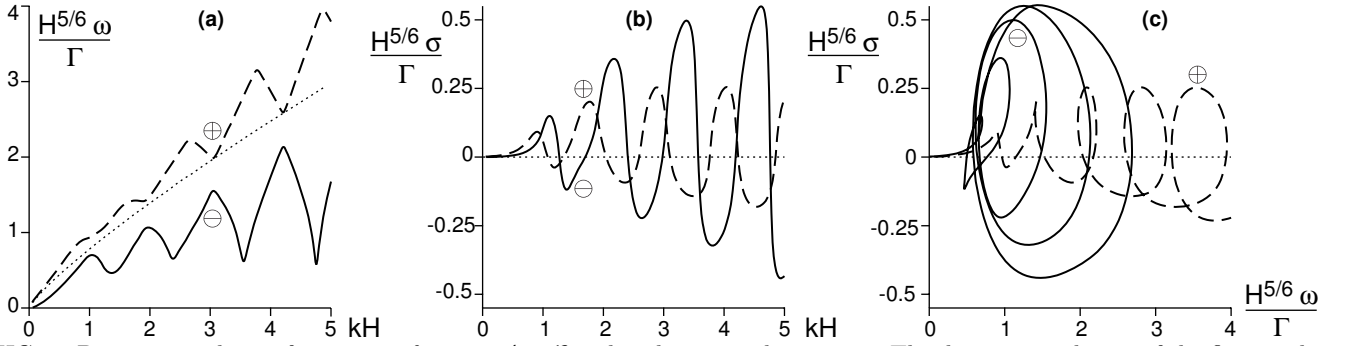


FIG. 2: Dispersion relation for $\mu = \tan \theta = 0.6$, $\mathcal{A} = \mathcal{B}$ and without any dissipation. The dispersion relation of the first mode in the absence of avalanche [14] is shown in dotted lines. The presence of the shear band gives rise to two branches, and no more, shown in solid \ominus and dashed lines \oplus . For each mode propagating upslope \uparrow with an angular frequency $\omega > 0$ and a growth rate σ , there exists a mode propagating downslope \downarrow with an angular frequency $-\omega$ and a growth rate $-\sigma$. (a) Relation between ω and k , both rescaled using the avalanche thickness H . (b) Relation between σ and k . (c) Relation between σ and ω .

elastic free energy of an isotropic granular packing can be written in the general form [14, 19]:

$$\mathcal{F} = E \left(\frac{2}{5} \mathcal{B} \delta^{5/2} + \mathcal{A} \delta^{1/2} u_{ij}^0 u_{ij}^0 \right) \quad (1)$$

where E is the material's Young's modulus, $\delta = -\text{Tr}(u_{ij})$ is the volumic compression and $u_{ij}^0 = u_{ij} + \frac{\delta}{3} \delta_{ij}$ the traceless strain tensor. \mathcal{A} and \mathcal{B} are two dimensionless elastic coefficients that characterise the material stiffness under shear and compression, respectively. It should be emphasised that \mathcal{F} is not supposed to describe the stress-strain curve obtained from a loading test, which consists of a series of elastic loadings and of plastic events. The derivation of the stress tensor yields:

$$\tau_{ij} = \frac{\partial \mathcal{F}}{\partial u_{ij}} = E \sqrt{\delta} \left(\mathcal{B} \delta \delta_{ij} - 2\mathcal{A} u_{ij}^0 + \frac{\mathcal{A} u_s^2 \delta_{ij}}{2\delta} \right) \quad (2)$$

with the sign convention corresponding to the equation of motion: $\rho \dot{\mathbf{U}} = -\nabla \bar{\tau} + \rho \mathbf{g}$. At equilibrium, the stresses simply balance gravity: $\tau_{zz} = \rho g \cos \theta z$ and $\tau_{xz} = \rho g \sin \theta z$. Introducing the volumetric compression

$$\delta_0 = \left(\frac{\rho g \sin \theta z}{2\mathcal{A}aE} \right)^{2/3} \quad \text{with} \quad a = \frac{1}{\mu} - \sqrt{\frac{1}{\mu^2} - \frac{5}{3} - \frac{\mathcal{B}}{\mathcal{A}}},$$

the strain tensor components take the form: $u_{xx} = 0$, $u_{zz} = -\delta_0$ and $u_{xz} = -a \delta_0$.

Disturbances – As the system is homogeneous both in time and along the x axis (but not in z), the solution of the linearized equations are a superposition of modes of the form: $\exp(ikx + i\omega t + \sigma t)$, where k is the wave-number, ω the angular frequency and σ the time growth rate. The vertical coordinate is rescaled by the wavenumber: $\zeta = kz$. The displacement field disturbance is normalized by the free surface position Z : $\mathbf{U} = (ZU(\zeta), ZW(\zeta))$. This gives a normalisation condition at the surface: $W(0) = 1$. To make the equations dimensionless, we introduce the parameter Γ , of dimen-

sion $[T^{-1}L^{5/6}]$, defined by:

$$\Gamma = \left[\frac{\sin \theta}{2a} \right]^{1/6} g^{1/6} \left(\frac{\mathcal{A}E}{\rho} \right)^{1/3} \quad (3)$$

The stress tensor disturbance is written under the form $\rho \Gamma^2 k^{2/3} \zeta T_{ij}(\zeta)$. The angular frequency is rescaled as $\sigma + i\omega = i \Gamma k^{5/6} \Omega$.

The linearization of the equations of motion leads to a set of four linear differential equations for $U(\zeta)$, $W(\zeta)$, $T_{xz}(\zeta)$ and $T_{zz}(\zeta)$:

$$\begin{aligned} U' &= -iW - \frac{6aiU + \zeta^{-1/3} \left((5 + 3\frac{\mathcal{B}}{\mathcal{A}} - a^2) T_{xz} - 2aT_{zz} \right)}{5 + 3\frac{\mathcal{B}}{\mathcal{A}} - 3a^2} \\ W' &= \frac{(1 - 3\frac{\mathcal{B}}{\mathcal{A}} + 3a^2) iU + 2\zeta^{-1/3} (aT_{xz} - T_{zz})}{5 + 3\frac{\mathcal{B}}{\mathcal{A}} - 3a^2} \\ T_{zz}' &= \Omega^2 W - iT_{xz} \\ T_{xz}' &= \Omega^2 U - iT_{xx} \quad \text{with} \quad T_{xx} = \frac{2(-1 - 6\frac{\mathcal{B}}{\mathcal{A}} + 6a^2) \zeta^{1/3} iU}{5 + 3\frac{\mathcal{B}}{\mathcal{A}} - 3a^2} \\ &\quad + \frac{6aT_{xz} + (-1 + 3\frac{\mathcal{B}}{\mathcal{A}} - 3a^2) T_{zz}}{5 + 3\frac{\mathcal{B}}{\mathcal{A}} - 3a^2} \end{aligned} \quad (4)$$

Some boundary conditions must be imposed to close this eigen-value problem. The interfacial stress must vanish at the free surface: $T_{zz} = T_{xz} = 0$. Across the frictional shear band, at $\zeta = kH$, the vertical displacement W and the stress components T_{zz} and T_{xz} are continuous. However, there is a discontinuity of the tangential displacement U , governed by the Coulomb relation $T_{xz} = \mu T_{zz}$. Finally, both components of the displacement vanish exponentially at infinity: $U(\infty) = W(\infty) = 0$.

The boundary value problem is solved numerically by a shooting method using a fourth order Runge-Kutta scheme. The superposition method is applied to get, for a given value of kH and Ω , the solution obeying the first three boundary conditions. We then apply the bisection root-finding algorithm to determine the relationship between Ω and kH . For this, we request U and W to vanish

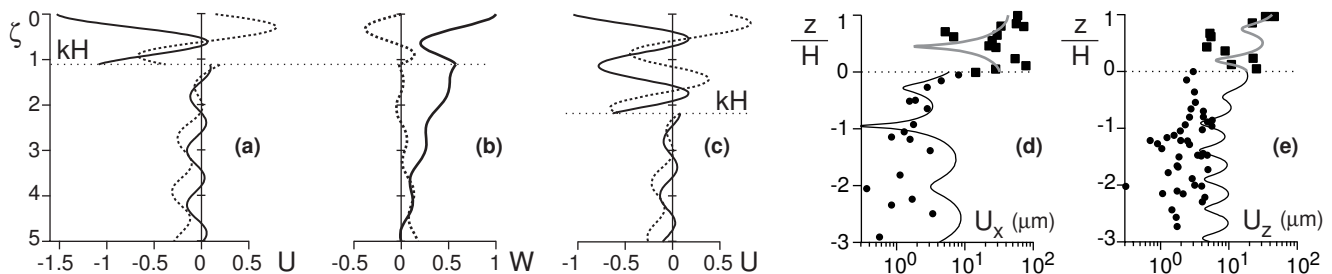


FIG. 3: **(a-b)** Profiles of the displacement (U and W) for the upward propagating mode associated to the first maximum of the growth rate (\ominus , $H^{5/6}\omega/\Gamma \simeq 0.68$ and $H^{5/6}\sigma/\Gamma \simeq 0.15$). **(c)** Profile $U(\zeta)$ for the second maximum of σ (\ominus , $H^{5/6}\omega/\Gamma \simeq 0.95$ and $H^{5/6}\sigma/\Gamma \simeq 0.36$). **(d-e)** Field measured profiles of the vibration amplitude along the x and z axis ($H \sim 35 \pm 10$ mm), at 3 m from the front. The first mode (a-b) is shown in solid line for the surface vibration amplitude $|Z| = \frac{g \cos \theta}{\omega^2}$ predicted in [4].

at a finite value of ζ and then let this value tend to infinity. Due to the structure of the equations, the uncertainty in $U(\zeta)$, $W(\zeta)$, $T_{xz}(\zeta)$ and $T_{zz}(\zeta)$ is on the order of the numerical precision times $\exp(\zeta)$. This limits in practice the value of kH to a maximum of $\simeq 6$.

Dispersion relation – The dispersion relation is presented in figure 2 for a typical avalanche slope, $\mu = \tan \theta = 0.6$. As such avalanches are close to the jamming transition, the ratio \mathcal{B}/\mathcal{A} should be close to, but smaller than, its critical value $1/\mu^2 - 5/3$; we have chosen here $\mathcal{B}/\mathcal{A} = 1$. In the absence of a shear band, there exists an infinite series of modes guided along the surface by gravity. The lowest mode gives rise, with a shear band, to two branches in the dispersion relation, noted \oplus and \ominus (fig. 2a); higher modes disappear. When σ is positive, the mode characterized by ω and k , which propagates up the slope (\uparrow), grows exponentially in time. By symmetry, there exists a mode propagating down the slope (\downarrow , k) that is damped with a rate $-\sigma$. Reciprocally, if σ is negative, the upward propagating mode decays but the downward propagating mode (\downarrow) is amplified. As a consequence, the system is unconditionally unstable at all wavenumbers. The maxima and minima of the growth rate σ are almost equally distributed in kH . In the geometric acoustics approximation (Fig. 1), guided modes are selected by the condition of constructive interference between plane waves as they bounce back and forth. As shown theoretically by [16, 17], an acoustic wave can be amplified coherently when reflected on a sliding frictional interface. The maximum energy gain is obtained for a particular angle of incidence. As the wave speed depends only on z , this condition determines a single ray, whatever the wavenumber. Altogether, there is a local maximum of the growth rate periodically in kH , for each constructive interference. The structure of the modes shown in figure 3 confirms this interpretation and show the oscillatory behaviour expected from the acoustic ray picture. In particular, the second maximum of σ (Fig. 3c) presents, above the frictional interface ($\zeta = kH$), one more oscillation than the first maximum (Fig. 3a). However, due to the heterogeneity of the system at the scale of the wavelength, the profiles also present non-oscillatory variations that prove the need for

a normal mode calculation using continuum mechanics.

Influence of dissipation – To address the selection of the most unstable wavelength, acoustic damping must be taken into account. This damping is the result of either the visco-elasticity of microcontacts, the linear viscous loss due to liquid films trapped in grain surface asperities, or to solid friction [20, 21]. Although it may depend on δ and ω , for simplicity we introduce a single dissipative time-scale ν and model the viscous stress as $\nu \frac{d}{dt} \left(\frac{\partial \mathcal{F}}{\partial u_{ij}} \right)$. The modified equation set is deduced from (4) by replacing Ω^2 with $\Omega^2/(1 + j\Omega\mathcal{N})$, where $\mathcal{N} = \Gamma H^{-5/6} \nu$. This damping stabilizes large wavelengths and even suppresses the instability when the dimensionless parameter \mathcal{N} is above a threshold value. So, for a given damping time, there is a threshold thickness above which the avalanche is unstable toward booming (Fig. 4). The most unstable modes belong to the upper branch, propagate

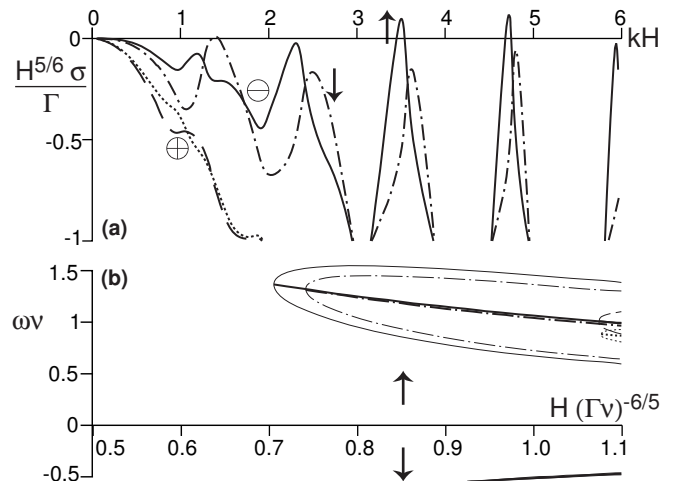


FIG. 4: **(a)** Growth rate σ as a function of kH taking dissipation into account ($\mathcal{N} = 1$). The branches correspond either to upward (\uparrow , \oplus in solid line and \ominus in dotted line) and downward (\downarrow , \oplus in dotted dashed line and \ominus in dashed line) propagating modes. **(b)** Bifurcation diagram showing the local maxima of the growth rate (bold lines) and the marginal stability curves (thin lines) as functions of $\mathcal{N}^{-6/5}$. The two most unstable modes are the third (dotted dashed line) and fourth (solid line) maxima of the branch \ominus and propagate upward (\uparrow).

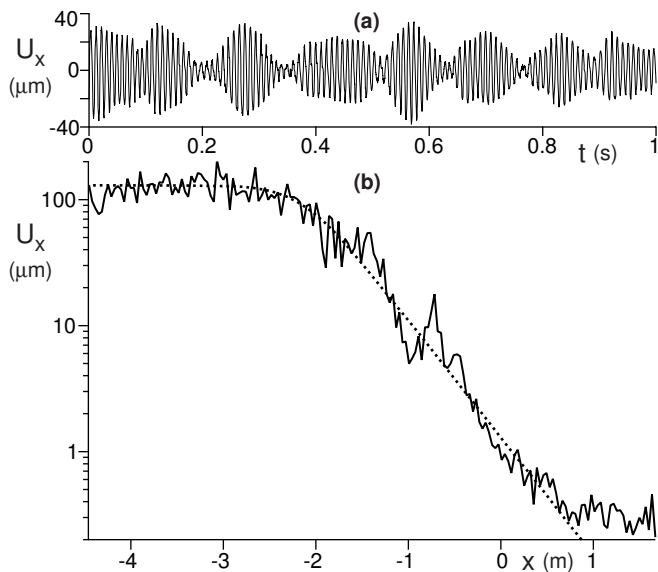


FIG. 5: **(a)** Typical displacement signal $U_x(t)$ measured with an accelerometer placed below a booming avalanche. Note the characteristic vibrato around a central frequency (here, $f = 107$ Hz). **(b)** Profile of the displacement amplitude along the avalanche axis. The dotted line shows the best fit by the amplitude equation expected for a convective instability: $\ell \partial_x U_x = U_x \left(1 - \frac{U_x^2}{U_\infty^2}\right)$, with $\ell = 2.1$ m and $U_\infty = 130$ μm .

up the slope and have neighboring frequencies. Near the threshold, the instability is thus convective and must lead to the spatial amplification of a doublet (Fig. 4), whose frequencies scale with the inverse of the dissipation time.

Field measurements – As predicted, a threshold height H for booming is observed in the field and the lab [5, 14]; it increases with humidity. The signals of accelerometers placed inside or below a booming avalanche systematically present a low frequency beating (Fig. 5a) which confirms the selection of several unstable modes of similar frequencies. By combining data obtained from 25 runs, we have been able to reconstruct a vibration profile across a booming avalanche (Fig. 3d-e). It presents a vibration node at mid avalanche height (like the first mode) and the displacement amplitude turns out to drop by one order of magnitude when crossing the interface between the flowing and static regions. Most of the spatial profiles recorded in the avalanche moving frame (Fig. 5b) show an exponential amplification of the vibration from the front to the core, as expected for a convective instability. In contrast to the theoretical situation, real avalanches are surrounded by a static sand region at the surface of which elastic waves can propagate in all directions. Even though downward propagating modes are damped in the flowing zone, the frequencies emitted at the rear of the avalanche are reinjected at the front through the sides.

It means that the avalanche is unstable *in time* towards modes exponentially growing in space.

Conclusion – We have shown that the shear band separating a booming avalanche from the static part of the dune induces a coherent amplification of guided elastic waves. This dynamical mechanism, demonstrated here for a particular constitutive relation, results in a linear instability, even at low Mach number. In conclusion, we wish to emphasize the generality of the result. As shown in [16, 17], the reflection of an elastic wave on a frictional interface results in energy pumping from shearing motion to coherent acoustic waves. This principle can probably be generalized and further applied to any thick interface inside which the shear stress increases with pressure [18]. The novelty, here, is to investigate a wave-guide whose boundary presents such an anomalous reflection. As in a LASER, the combination of a cavity with an acoustic amplifier results in a spontaneous emission of coherent waves, if the energy loss is sufficiently low.

-
- [1] C. Carus-Wilson, *Nature* **44**, 322 (1891).
 - [2] J.H. Poynting, *Nature* **77**, 248 (1908).
 - [3] P.K. Haff, *Am. Sci.* **74**, 376381 (1986).
 - [4] B. Andreotti, *Phys. Rev. Lett.* **93**, 238001 (2004).
 - [5] S. Douady *et al.*, *Phys. Rev. Lett.*, **97**, 018002 (2006).
 - [6] Vriend *et al.* *Geophys. Res. Lett.* **34**, L16306 & **35**, L08306 (2008). Note that the word *resonance* is incorrectly used there for *guided wave critical angle*.
 - [7] F. Nori, P. Sholtz, and M. Bretz, *Sci. Ame.* **277**, 84 (1997).
 - [8] D. Goldsack, M. Leach and C. Kilkenny, *Nature* **386**, 29 (1997).
 - [9] R.A. Bagnold, *Proc. Roy. Soc. London, Ser. A* **295**, 219 (1966).
 - [10] S. Douady, B. Andreotti, A. Daerr, and P. Cladé, *C.R. Physique* **3**, 177-186 (2002).
 - [11] A.J. Patitsas, *Sci. Jou. Int.* **2**, 1 (2008).
 - [12] L. Bonneau, B. Andreotti, and E. Clément, *Phys. Rev. Lett.* **101**, 118001 (2008).
 - [13] V.E. Gusev, V. Aleshin and V. Tournat, *Phys. Rev. Lett.* **96**, 214301 (2006).
 - [14] L. Bonneau, B. Andreotti, and E. Clément, *Phys. Rev. E* **75**, 016602 (2007).
 - [15] G.D.R. Midi, *Eur. Phys. Jour. E* **14**, 341 (2004).
 - [16] M. Nosonovsky, G.G. Adams, *Int. J. Ing. Sci.*, **39**, 1257 (2001).
 - [17] C. Caroli and B. Velický, *Phys. Rev. E* **67**, 061301 (2003).
 - [18] A. Furukawa and H. Tanaka, *Nature* **443**, 434-438 (2006).
 - [19] Y. Jiang and M. Liu, *Phys. Rev. Lett.* **91**, 144301 (2003).
 - [20] T. Baumberger, P. Berthoud and C. Caroli, *Phys. Rev B* **60**, 3928 (1999).
 - [21] Th. Brunet, X. Jia and P. Mills, *Phys. Rev. Lett.* **101**, 138001 (2008).